Development and Evaluation of a Portable MR Compatible Haptic Interface for Human Motor Control

Ildar Farkhatdinov, Arnaud Garnier, Etienne Burdet

HAL Id: hal-01175926

https://hal.science/hal-01175926

Submitted on 13 Jul 2015

Development and Evaluation of a Portable MR Compatible Haptic Interface for Human Motor Control

Ildar Farkhatdinov[1]   Arnaud Garnier[1,2]   Etienne Burdet[1]

Abstract— This paper presents the development and evaluation of an MR compatible haptic interface for human motor control studies, which can be easily installed and removed from the scanner room. The interface is actuated by a powerful shielded DC motor located 2.1 m away from the 3T MR scanner. Rotational movements are transmitted to a subject's wrist through preloaded cable transmission which drives the handle unit. The handle of the interface is designed to be adjustable to different hands size, enabling comfortable and natural wrist movements. The nominal achievable wrist torque of the interface is up to 2Nm. The interface is easily transportable due to its design characteristics. A dynamic model of the interface is presented and identified for position and torque control modes. Phantom MR compatibility test in clinical environment showed that the interface is compatible with strong magnetic field and radio frequency emission and its operation does not affect the quality of MR images.

I. INTRODUCTION

Force feedback devices have provided powerful tools for investigation of sensorimotor control and learning in humans [1], [2], [3], [4]. Instrumentation of haptic interfaces in magnetic resonance (MR) imaging can be used to study neural mechanisms of human motor control. The application of novel materials and techniques, as well as improvements of MR technology, enabled deployment of mechatronic systems in the clinical MR environments. A detailed survey of MR compatible actuation and sensing techniques can be found in [5], [6]. Next paragraphs briefly review some of previously developed interfaces and analyze the needs for an MR compatible force feedback interface.

An MR compatible master-slave robotic system with hydraulic transmission was presented in [7], [8]. A magnetically inert actuator using a direct drive to power the hydraulic circuitry and a modular set of position and force/torque sensors were used for wrist actuation. However, that interface was built on a big metal frame which together with the usage of hydraulic systems made the setup bulky and difficult to remove in case of hazards. A 1-DOF haptic interface was developed in [9], which was made of two coils that produced a force induced by the static magnetic field of the scanner. However such an interface is difficult to control in a reliable and robust way. In order not to affect the imaging quality, the generated torques were limited up to 4 Nm at a 1 m distance from the scanner's focal point. A detailed investigation of electromechanical cable MR compatible transmission is presented in [10]. Cable transmission allowed to locate electric motors at a safe distance from the scanner. Dynamic behaviour of transmissions with different cable length was investigated and stable interaction was achieved with the transmission up to 9 m length. In [11] a shielded actuation system located inside the MR room was presented. Shielded conventional electromagnetic motor with long rigid rod was used to transmit rotational movements to a subject's hand enabling control of pronation/supination movements. In [12] a pneumatic based human ankle movement interface for MR imaging studies was presented. Electro-pneumatic control was used to move one or both feet, however only open loop control was used which limited the applications of the system. A 3-DOF MR compatible haptic interface based on four-bar kinematics with a long end-effector link was developed in [13]. DC motors which were used to actuate the system and all electronics were shielded and located at a safe distance from the scanner. The interface was used for motor control studies during interaction with virtual reality. In [14] MR safe wrist stimulating interface for neonates was developed. The interface helped to reliably identify the cortical activity associated with both active and passive movements.

Most of the haptic interfaces cited above are conceived to investigate human movements involving several joints, making it difficult to analyze muscle activity systematically. In contrast, the dual wrist haptic interface Hi5 developed in our group [15] to study the bimanual wrist flexion/extension provides a simple measurement of muscle electromyography (EMG). This enables us to analyse the motor commands precisely by focusing on one group of antagonist muscles, e.g. flexor carpi radialis and extensor carpi radialis longus. The Hi5 handles ergonomic design minimizes the confound of fingers flexion.

In this paper we present the development of an MR compatible haptic interface which takes advantages of the Hi5 device kinematic arrangements, enabling human motor control studies combining haptic interaction, EMG and MRI. The interface should be MR compatible with magnetic field of up to 3T and be adaptable to scanners with different geometries. The overall system should be easily transportable and easily removable if any interruption of the experiment is required. Last but not least, studying the wrist flexion/extension movement is favorable for fMRI studies of human motor control as it will minimize head motion artifacts.

*I. Farkhatdinov and A. Garnier contributed equally to this paper.

[1]All authors are with dept. of Bioengineering, Imperial College of Science, Technology and Medicine, South Kensington Campus, London, United Kingdom, SW72AZ. {i.farkhatdinov,e.burdet}@imperial.ac.uk.

[2]Arnaud Garnier is also with École Polytechnique Fédérale de Lausanne, Switzerland.

II. REQUIREMENTS FOR MR COMPATIBILITY

A strong magnetic field and radio frequency (RF) waves pose compatibility issues and safety hazard for the design of haptic systems to be used with MR scanners. Safety of MR compatible devices has been intensively studied, however due to complex physical nature of MR technology most of safety guidelines are qualitative or described with some approximations [16], [17].

Magnetic forces. A static magnetic field causes strong forces on ferrous materials which pose a safety problem as an object can be quickly pulled into the bore of the scanner; this can damage equipment, and also fatally injure a person laying inside the bore [18], [19]. Thus the usage of ferromagnetic objects should be avoided, or they should be placed at a safe distance and firmly fixed. The magnetic force F_m acting on ferrous objects in a background magnetic field can be calculated as

$$F_m = -\nabla(U_m) = \nabla(m \cdot B) \tag{1}$$

where m is the magnetic moment of the ferrous object and B the flux density of the magnetic field [20]. To approximation the maximal possible magnetic force, we consider that the ferrous object is placed along the scanner's z-axis. We also assume that the magnetic field due to the magnetisation of the ferromagnetic element is saturated to M_s, such that the maximum induced magnetic moment is

$$m_{max} = M_s V = \frac{B_s V}{\mu_0} \tag{2}$$

with the volume of the ferromagnetic element V, flux of the magnetic field inside the ferromagnetic element B_s, and magnetic constant $\mu_0 = 4\pi \cdot 10^{-7}$ N/A^2. Using (1) and (2) we can express the magnetic force along the z-axis of the scanner as

$$F_{mz} = m_{max} \frac{\partial B_z}{\partial z} = \frac{B_s V}{\mu_0} \frac{\partial B_z}{\partial z} \tag{3}$$

where B_z is the scanner's magnetic field flux density at a certain point along the z-axis of the scanner. Fig. 1 shows the magnitude of this magnetic field flux density over the scanner's bore z-axis which should be used for magnetic force calculation. The ratio of magnetic force acting on the ferromagnetic part with its weight is used as a measure to evaluate potential risks of the ferrous part attraction by the scanner [20]:

$$\beta_F \triangleq \frac{|F_m|}{|F_g|} \tag{4}$$

with F_g the gravity forces. When $\beta_F < 1$ the gravity is stronger than the magnetic force and thus the risk that the part is flying is reduced. In [20] $\beta \equiv 0.1$ was introduced as a safe limit. In reality this magnetic static field can also interfere with sensors and electromagnetic motors. Finally an electro-conductive material moving in this field will experience a magnetic gradient that causes an electric field thus inducing currents, heat, electromagnetic and magnetic fields. This is potentially dangerous for a human subject and
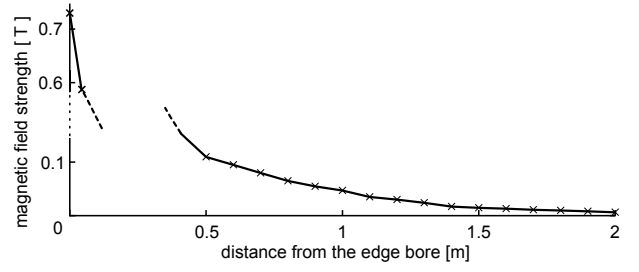

Fig. 1. Simulation of static field generated by a 3T scanner: the field substantially decreases over its distance to the scanner. These data are adapted from [11].

adds magnetic field inhomogeneities as well as RF noise to the measurement.

Radio frequency interaction. RF waves in MR environments have a frequency above 100 MHz, which is a source of heat when resonating inside an electro-conductive component that can lead to human burn injuries [21]. These waves can also bring electromagnetic interference (EMI) and affect sensors or signals inside transmission lines. Finally, electrically active components inside the MR room will create EMI which will corrupt MR signals adding distortion, speckles and noise to the scanned images. Therefore EMI of electronic devices used in the MR room should be minimized and filtered. In [22] it is suggested that at least 80 dB of emitted by the electronic devices EMI should be attenuated. Therefore the Faraday cages are used to shield all electronic devices. The direct attenuation loss of the wave against the walls of the cage occurs through the absorption A_{dB} and reflection. The reflection takes place for a plane wave which is not relevant here, as the EMI source is close to the barrier. Therefore only the absorption is considered here. The attenuation due to absorption can be calculated as in [23]:

$$A_{dB} = 0.13t\sqrt{f\sigma_r\mu_r} \tag{5}$$

with t the barrier thickness in cm (thickness of the Faraday cage walls), f the frequency to filter, σ_r the relative conductivity to copper (σ_r=0.6 for aluminium), and μ_r the relative permeability relative to copper (μ_r=1 for aluminium). The size of the openings in the Faraday cage should be taken into consideration for EMI isolation as well. If the size of the opening is close to 1/2 of the wavelength λ, it behaves as an antenna which re-radiates behind the shield. In general, one takes $\lambda/10$ to determine the maximum size of the openings.

III. MECHATRONIC DESIGN

A general view of the proposed MR compatible wrist interface is shown in Fig. 2. The vertical aluminium frame supports the weight of the interface. The horizontal frame provides a rigid connection between the actuation system and the wrist interface. The fasteners used to connect the frames are made of brass or plastic. The actuation system consists of a DC motor with an optical encoder and a cable transmission. The wrist interface (handle unit) is made of plastic materials.
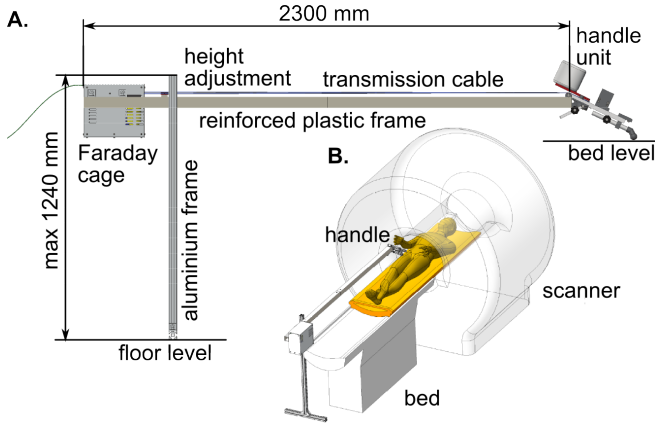
Fig. 2. Overview of the haptic interface design (CAD). **A**: Side view of the interface and its frame. **B**: A user during wrist interaction experiment in MR room using the designed interface.
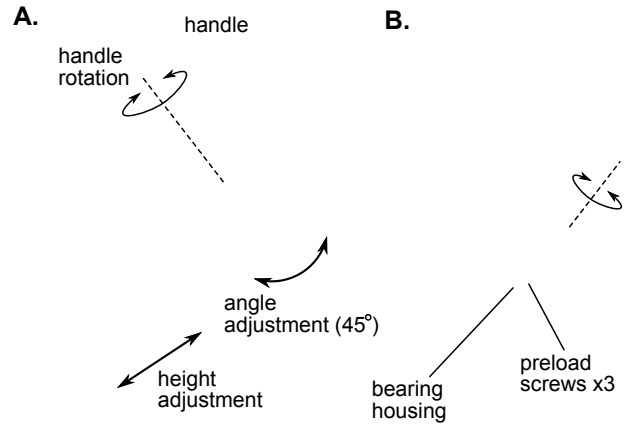

Fig. 3. Handle unit and its mechanisms CAD drawing. **A.** General view of the handle unit with adjustable geometry. **B.** Bottom view of the bearing housing and preload regulation.

Main frame. The frame was designed to be easily removable following the safety requirement of patient/user emergent evacuation. The frame is rigid enough to handle a 2.1 m cable transmission and its preload. The height of the frame is adjustable, so that it can be used for different types of scanners. The frame does not contain any ferromagnetic materials and its design enables fast assembling, disassembling and easy transportation. The vertical frame is made of aluminium. The actuator and the handle are linked by a 2.1 m long horizontal combined profile made of nonconductive glass reinforced plastic which is easily splittable into two parts for transportation.

The handle unit design is presented in Fig. 3. The main part to which each component is attached was milled from nylon to insure rigidity of the system. Two polymer ball bearings (Xiros, IGUS) are used to reduce the friction of the handle rotation. However, since the bearings have a plastic cage there is a significant angular and axial backlash which is removed by housing the bearings together with "duplex back to back" arrangement in which the inner and outer rings are clamped together with preload to attain greater axial and radial rigidity.

Actuation. To actuate the interface a DC motor boxed together with control electronics and batteries in a Faraday cage is used. The reduction ratio is chosen to be 2 in order to achieve required handle torques $\tau_h = 1.6$ Nm (similar to the nominal torque of Hi5 interface), with a DC motor Maxon 353301 with the highest nominal torque of 0.86 Nm. Optical encoder (Avago HEDR) with 3600 quadrature counts per revolution with resolution of $0.025°$ is attached to the motor shaft to measure the angular position.

Cable transmission. A low-weight high-strength 2 mm diameter cable made of polyethylene fiber with a young modulus of 172 GPa is used for rotational motion transmission (Dyneema cable). The ends of the cable are attached to the motor and handle pulleys with adjustable plastic screws, such that the motor pulley can synchronously drive the handle pulley. The diameters of the motor and the handle pulleys are 30 and 60 mm, respectively. To avoid nonlinearities such

as backlash, the cables are preloaded with the help of an additional movable pulley mounted with a plastic bearing to the horizontal frame. As a result, the path of the transmission cable is constrained with this movable pulley, which makes it possible to control tension of the cable easily.

Without sufficient tension preload during operation one side of the cable will be strained and the other will be loose. To avoid this the tension forces of both sides of the cable should be positive and directed away from the motor pulley: $F_1 > 0$ and $F_2 > 0$ (see Fig. 4A). The two forces F_1 and F_2 can be expressed as

$$F_1 = T + \Delta F > 0\,, \qquad F_2 = T - \Delta F > 0 \quad (6)$$

with cable transmission preload tension T, and force ΔF caused by the motor torque τ_m. The motor torque can be expressed as:

$$\tau_m = \frac{D_m}{2}(F_1 - F_2) = D_m \Delta F\,, \quad (7)$$

where D_m is the motor pulley diameter. Then from (6) and (7), the minimal required tension is

$$T > \frac{\tau_m}{D_m}\,, \quad (8)$$

which means that for a maximal motor torque of 3.8 Nm the minimum preload is 127 N. We verified that the maximal wrist torque at Hi5 interface was ≈2.7 Nm leading to required preload force of 45 N. The maximal achievable wrist torque of our interface was up to 7.6 Nm. At a practical level, as no torque sensor is mounted, one would apply the maximum torque for the experiment and increase the preload until the loose thread of cable transmission is stretched.

Control and power. The motor is controlled by a Maxon ESCON 409510 current driver. A 16 bit data acquisition card (DAQ NI USB-6211) forms reference current commands for the motor controller and transmits the motor's encoder and current values to the control computer (laptop) using an optical USB cable (M2-100-10 OPTICIS). For MRI compatibility the motor, its controller and DAQ card, batteries
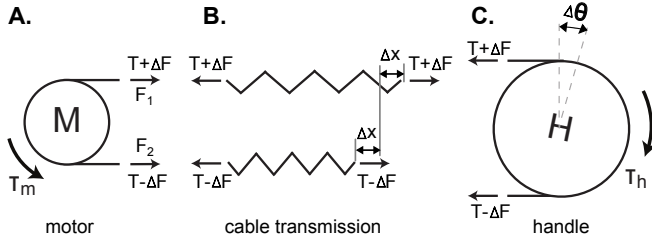
Fig. 4. Simplified dynamic model of the motor side (**A**), cable transmission (**B**) and handle (**C**).

are installed inside the Faraday cage while the control computer is located outside the scanner's room. Communication between the DAQ and control computer is done via an optical USB cable. Three batteries of $7.4\ V$ and $5\ A \cdot h$ are connected in series ($22.2\ V$ and $111\ W \cdot h$). Calculations showed that with this power supply the interface can run for more than 3 hours. Usage of batteries and optical communication cable facilitates shielding and make the system easily adaptable to different MR rooms. An application developed in NI Labview was used to implement different control modes, i.e. open-loop torque control, closed-loop position tracking, interaction with virtual wall.

Ergonomics and safety. An important issue was to design a comfortable, adjustable and safe wrist handle and related mechanisms. A user should not feel any discomfort during interaction with the device, therefore it was important to find a good position and orientation of the arm as well as the location and workspace of the wrist in a very limited space of the scanner's bore. Besides, the wrist flexion/extension should remain natural, painless and should not cause any significant movements of other body parts, which is critical for brain imaging studies [24]. To fulfill these ergonomic requirements an option to adjust inclination of the handle's rotational axis in the vertical plane was added (Fig. 3A). Additionally, the height of the forearm support was made adjustable in order to provide the interface with flexibility to adapt to users with different arm length. The handle design was similar to the ergonomic handle developed for the Hi5 haptic interface, which enables comfortable contact between a users palm and fingers and the interface during the wrist motion [15]. Mechanical safety stops were used to limit the workspace of the wrist to $\pm 40°$. At software level safety was implemented by limiting the maximum produced torque. The proposed design made it possible to minimize the time required to assemble the interface for usage in MR environment to less than 10 minutes, which is beneficial for MR imaging studies which can be costly and time constrained.

MR compatibility. The magnetic static field B_0 of the scanner to be used in the studies is 3 T which can lead to potentially dangerous physical interactions with a 250 W DC-motor used in the interface. The magnetic field produced by the motor can affect the homogeneity of the scanner's field. In [20] it was shown that the magnetic force for a 90 W DC motor is smaller than the scanner's resolution

at a distance more than 30 cm from the motor. Knowing that the motor's magnetic field decreases significantly with the distance and following the design approach from [20], our estimations showed that if our motor is placed about 2 m away from the scanner bore, then it will not affect the scanner's magnetic field homogeneity.

Second MR compatibility requires checking magnetic forces acting on ferrous parts of the interface. The scanner's static magnetic field exerts a magnetic force on the DC-motor which is the biggest ferrous part of the interface (motor weights 2.1 kg). Since the exact materials composition of the motor are unknown we considered the worst scenario representing the motor as an iron ball with material density ρ=7.8 gr/cm^3 and volume V=266.7 cm^3. The magnetic flux inside the motor is saturated to B_s=2.2 T. We also assumed that the motor is fixed along the scanner z-axis at the actual distance of 2.1 m from the edge of the bore where, from Fig. 1, the magnetic field is 5 mT and its gradient is 15 mT/m. Using (2)-(4) we calculated the magnetic force acting on the motor F_{mz}=7 N and the ratio of this force to the weight of the motor $\beta_F = 0.3$. The motor is enclosed in a 2.5 kg Faraday cage which reduces the factor β_F to 0.14. Furthermore, the motor and the Faraday cage are firmly attached to a frame with a total mass of 10 kg which reduces β_F to 0.07. These calculations show that the proposed haptic interface design with selected powerful DC motor can be safely used in the MR room if the motor is not closer than 2 m from the edge of the bore.

To filter the EMI produced by the interface electronic components we built the Faraday cage from 3 mm thickness aluminium sheets. Calculated with (5) EMI absorption is 1000 dB which satisfies the requirements of EMI filtering. The size of the maximum opening in the cage was 7 cm which is smaller than 23.6 cm, the permissible opening's size for RF of 127 MHz.

IV. DYNAMICS IDENTIFICATION

Compliance. The interface has some compliance stemming from the cable the cable and the plastic mechanism of the handle. To evaluate the compliance, we mechanically blocked the handle's shaft and attached a (ATI SI-145-5) torque sensor to it. The experimental angular stiffness, k_θ, can then be calculated as

$$\frac{1}{k_\theta} = \left.\frac{\theta_m}{\tau_m}\right|_{\theta_h fixed} = \left.\frac{\theta_m}{r \cdot \tau_h}\right|_{\theta_h fixed} \tag{9}$$

with θ_m, θ_h, τ_m, τ_h the angles and torques of the motor and the handle, respectively, and the reduction ratio $r = 2$. In several trials we measured angular deflection from the motor's encoder and the corresponding torques applied to the blocked handle. Linear regression applied to the measured data led to an estimated compliance of 2.21 deg/Nm.

Linear dynamics identification. To model dynamics of the interface we assume that the motor and the handle sides are linear second order mechanical systems with inertia J_m, J_h and viscous friction b_m, b_h with indexes m and h standing for the motor and handle parameters. Two systems are

connected with transmission cable via attachments to motor pulley with diameter D_m and to handle pulley with diameter D_h. Simplified dynamic schematics is shown in Fig. 4. In the frequency range of interest, 0-20 Hz, the transmission can be considered as two massless springs each characterized by stiffness k and preload force T. Then, the equations of motion of the motor and the handle are expressed as

$$
\begin{aligned}
J_m \ddot{\theta}_m(t) &= \tau_m(t) - F(t)D_m - b_m \dot{\theta}_m(t), \\
J_h \ddot{\theta}_h(t) &= \tau_h(t) - F(t)D_h - b_h \dot{\theta}_h(t),
\end{aligned} \quad (10)
$$

where $\theta_m(t)$ and $\theta_h(t)$ are angular positions of the motor and the handle, respectively; $F(t)$ is tension of the transmission cable caused by the motor torque $\tau_m(t)$; the handle is subject to the user's input $\tau_h(t)$ which due to compliance of the system leads to an angular difference $\Delta\theta$. Then the position of the handle is related to position of the motor as

$$
\theta_h(t) = \frac{D_m}{D_h}\theta_m(t) + \Delta\theta(t), \quad (11)
$$

where $\Delta\theta(t)$ can be expressed via transmission compliance (spring deformation) or cable tension:

$$
\Delta\theta(t) = \frac{2\Delta x(t)}{D_h} = \frac{2F(t)}{kD_h}. \quad (12)
$$

The transfer function is computed from the Laplace transform of (10)-(12) as expressed in (13).

We obtained the transfer function of (13) which models continuous open loop dynamics of the interface. To identify the dynamics we considered the closed loop system stabilized by discrete position PD-regulator at sampling time 5 ms (sampling is limited by USB communication). The discrete transfer function to identify becomes:

$$
\frac{\Theta_y(z)}{\Theta_u(z)} = G(z) = \frac{G_r(z)G_0(z)}{1 + G_r(z)G_0(z)} \quad (14)
$$

with $\Theta_y(z)$ and $\Theta_u(z)$ respectively the measured and command angle and $G_r(z)$ the transfer function of the PD controller: $G_r(z) = K_p + K_d \frac{1-z^{-1}}{T_s}$. From (14) the transfer function's estimation of the mechanical system becomes:

$$
\hat{G}_0(z) = \frac{G(z)}{G_r(z)(1 - G(z))}. \quad (15)
$$

The identification of $G(z)$ is based on the frequency analysis of the measured output signal $\theta_m(t)$ relative to an input command $\tau_m(t)$. Several angular position step inputs of $20°$ were applied with the PD coefficients K_p=0.077 Nm/deg and $K_d = 3.1$ Nm·s/deg. The system was identified with the help of the Matlab toolbox for the operational frequency range 0-15 Hz. Fig. 5A shows the Bode diagram of the chosen identified system. The transfer function of the identified model is

$$
G(z) = \frac{0.1269z^3 - 0.2973z^2 + 0.2646z - 0.08673}{z^4 - 3.357z^3 + 4.374z^2 - 2.614z + 0.605}. \quad (16)
$$

Then, substitution of $G(z)$ in (15) yields the identified open loop dynamics of the haptic interface.
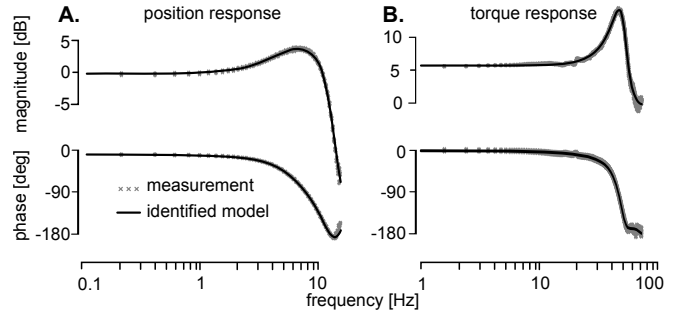

Fig. 5. System identification results. **A.** Frequency response for closed loop position control with best fit transfer functions. **B.** Frequency response of torque control with best fit transfer function.
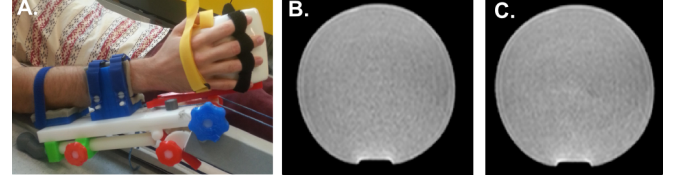

Fig. 6. **A.** A subject during the motor control test; the adaptable wrist inclination and forearm length enable natural movement. **B-C.** Phantom scans of MR compatibility test: the (**B**) scan is done with the interface off, SNR=28.3 dB; the (**C**) scan with the interface on, SNR=28.6 dB.

Torque control response. Next we identified the torque bandwidth of the interfaces. For this procedure, the set-up with blocked handle and attached torque sensor as it was used for compliance identification tests, was used with a cable preloaded to 50 N. A set of input torque step commands of 1.2 Nm was applied to the motor controller and response of the measured torque τ_h at the blocked handle was recorded. After applying Fourier transform and using the Matlab identification toolbox the following transfer function was obtained

$$
G_\tau(z) = \frac{\tau_h(z)}{\tau_m(z)} = \frac{2.007z^3 + 0.2405z^2}{z^4 - 0.3474z^3 + 0.7029z^2 - 0.2083z + 0.08962}. \quad (17)
$$

Fig. 5B shows the torque control frequency response and Bode diagram of the identified transfer function $G_\tau(z)$.

System identification tests showed that the described haptic interface provides sufficient bandwidth for motor control studies. Identified position and torque frequency responses can be used for dynamic compensation and advanced control design in future developments.

V. EVALUATION

To evaluate the ergonomics of the designed interface we asked five subjects to use the interface for 10 minutes of pre-programmed various motor control tests such as tracking position control, interaction with virtual wall, etc. No discomfort or pain was reported by the subjects. Fig. 6A shows a subject during the test. The test was approved by the ethics committee at Imperial College London.

MR compatibility tests were carried out with a scanner Philips Achieva 3.0 T TX located at St Thomas hospital, London, UK. No magnetic pulling force was perceived during the interface preparation and set-up in the MR

$$G_0(s) = \frac{\mathcal{L}\{\theta_m(t)\}}{\mathcal{L}\{\tau_m(t)\}}\bigg|_{\tau_h(t)=0} = \frac{\frac{-2J_h}{kD_h}s^2 - \frac{2\nu_h}{kD_h}s + D_h}{\frac{-2J_mJ_h}{kD_h}s^4 - \frac{2(J_m\nu_h + J_h\nu_m)}{kD_h}s^3 + (J_mD_h - \frac{2\nu_m\nu_h}{kD_h} + \frac{D_m^2}{D_h}J_h)s^2 + (\nu_mD_h + \frac{\nu_hD_m^2}{D_h})s} \quad (13)$$

room which confirms the low magnetic attraction force calculations. During MR compatibility tests the motor was controlled by a microcontroller located inside the Faraday cage. Current steps of ± 2 A equivalent to 1.2 Nm were applied to the motor. An echo planar image sequence was recorded on a phantom test (a cylindrical tank filled with an aqueous solution). During imaging 24 z-slices with 256×256 resolution were taken for the cases when the interface was running and off. As it is shown in Fig. 6B-C no distortion of the images was observed linked to field inhomogeneity or speckles/strips artifacts related to RF interference. Statistical comparison of the images did not show any significant differences.

VI. CONCLUSION

This paper presented the development and evaluation of an MR compatible haptic interface for human motor control studies. The proposed ergonomic design of the wrist actuation interface facilitates employment of neat hand muscle EMG measurements in addition to haptic and MR imaging techniques. The system is low cost, easy to transport and set up and can be adapted to different scanners with magnetic fields up to 3 T. The interface was successfully tested in a 3T MR scanner. It proved to be safe and did not degrade the quality of MR imaging. Designed control system runs at a sampling frequency of 200 Hz and dynamic identification tests showed that the interface provides sufficient bandwidth for human motor research experiments. Two such interfaces will be used to study the neural mechanisms of bimanual control and of motor interaction between two subjects with at least one of them within the bore of an MR scanner.

ACKNOWLEDGMENT

REFERENCES

[1] E. Burdet, R. Osu, D. W. Franklin, T. E. Milner, and M. Kawato, "The central nervous system stabilizes unstable dynamics by learning optimal impedance." *Nature*, vol. 414, no. 6862, Nov. 2001.

[2] F. Mussa-Ivaldi, N. Hogan, and E. Bizzi, "Neural, mechanical, and geometric factors subserving arm posture in humans," *J. Neurosci.*, vol. 5, no. 10, 1985.

[3] I. Howard, J. Ingram, and D. Wolpert, "A modular planar robotic manipulandum with end-point torque control." *J. of Neuroscience methods*, vol. 181, no. 2, July 2009.

[4] J. Klein, N. Roach, and E. Burdet, "3DOM: a 3 degree of freedom manipulandum to investigate redundant motor control." *IEEE T on Haptics*, vol. 7, no. 2, Jan. 2014.

[5] R. Gassert, D. Chapuis, H. Bleuler, and E. Burdet, "Sensors for Applications in Magnetic Resonance Environments," *IEEE/ASME T. on Mechatronics*, vol. 13, no. 3, June 2008.

[6] R. Gassert, A. Yamamoto, D. Chapuis, L. Dovat, H. Bleuler, and E. Burdet, "Actuation methods for applications in MR environments," *Concepts in Magnetic Resonance Part B: Magnetic Resonance Engineering*, vol. 29B, no. 4, Oct. 2006.

[7] R. Gassert, R. Moser, E. Burdet, and H. Bleuler, "MRI/fMRI-compatible robotic system with force feedback for interaction with human motion," *IEEE/ASME T. on Mechatronics*, vol. 11, no. 2, Apr. 2006.

[8] R. Moser, R. Gassert, E. Burdet, L. Sache, H. Woodtli, J. Erni, W. Maeder, and H. Bleuler, "An MR compatible robot technology," in *Proc. of IEEE Int. Conf. on Robotics and Automation*, vol. 1, 2003.

[9] R. Riener, T. Villgrattner, R. Kleiser, T. Nef, and S. Kollias, "fMRI-compatible electromagnetic haptic interface." *Proc. of Ann. Int. Conf. of the IEEE Eng. in Medicine and Biology Soc.*, vol. 7, Jan. 2005.

[10] D. Chapuis, R. Gassert, G. Ganesh, E. Burdet, and H. Bleuler, "Investigation of a cable transmission for the actuation of MR compatible haptic interfaces," in *Proc. of IEEE Int. Conf. on Biomed. Robotics and Biomechatronics*, 2006.

[11] M. Hara, J. Duenas, T. Kober, D. Chapuis, O. Lambercy, H. Bleuler, and R. Gassert, "Design and compatibility of a high-performance actuation system for fMRI-based neuroscience studies," in *Proc. of IEEE/RSJ Int. Conf. on Intelligent Robots and Systems*, Oct. 2010.

[12] G. Belforte and G. Eula, "Design of an active-passive device for human ankle movement during functional magnetic resonance imaging analysis," *Proc. of the IMechEng., Part H: J. of Eng. in Medicine*, vol. 226, no. 1, Oct. 2011.

[13] S. Menon, G. Brantner, C. Aholt, K. Kay, and O. Khatib, "Haptic fMRI: combining functional neuroimaging with haptics for studying the brain's motor control representation." *Proc. of Ann. Int. Conf. of the IEEE Eng. in Med. and Biology Soc.*, Jan. 2013.

[14] A. G. Allievi, A. Melendez-Calderon, T. Arichi, A. D. Edwards, and E. Burdet, "An fMRI compatible wrist robotic interface to study brain development in neonates." *Annals of biomed. eng.*, vol. 41, no. 6, June 2013.

[15] A. Melendez-Calderon, L. Bagutti, B. Pedrono, and E. Burdet, "Hi5: A versatile dual-wrist device to study human-human interaction and bimanual control," in *Proc. of IEEE/RSJ Int. Conf. on Intelligent Robots and Systems*, Sept. 2011.

[16] G. Schaefers and A. Melzer, "Testing methods for MR safety and compatibility of medical devices." *Minimally invasive therapy & allied technologies*, vol. 15, no. 2, Jan. 2006.

[17] G. Schaefers, "Testing MR safety and compatibility: an overview of the methods and current standards." *IEEE eng. in med. and biology magazine*, vol. 27, no. 3, Jan. 2008.

[18] J. McConnell, *Index of Medical Imaging*. Oxford, UK: Wiley-Blackwell, May 2011.

[19] F. G. Shellock, "Policies, guidelines, and recommendations for MR imaging safety and patient management," *J. of Magnetic Resonance Imaging*, vol. 1, no. 1, Jan. 1991.

[20] N. Yu, R. Gassert, and R. Riener, "Mutual interferences and design principles for mechatronic devices in magnetic resonance imaging." *Int. J. of computer assisted radiology and surgery*, vol. 6, no. 4, July 2011.

[21] M. F. Dempsey, B. Condon, and D. M. Hadley, "Investigation of the factors responsible for burns during MRI." *J. of magnetic resonance imaging*, vol. 13, no. 4, Apr. 2001.

[22] H. Vinegar and J. Taylor, "US Patent: Scan room for magnetic resonance imager," Mar. 1987.

[23] Report, "Electromagnetic shielding guidance: online at www.jacquesdubois.com," 2014.

[24] Z.-M. Li, L. Kuxhaus, J. A. Fisk, and T. H. Christophel, "Coupling between wrist flexion-extension and radial-ulnar deviation." *Clinical biomechanics*, vol. 20, no. 2, Feb. 2005.